Letter

Electrostatic Collapse of Intrinsically Disordered Acid-Rich Protein Is Sensitive to Counterion Valency

Barbara P. Klepka, Radost Waszkiewicz, Michał Wojciechowski, Agnieszka Michaś, and Anna Niedzwiecka*
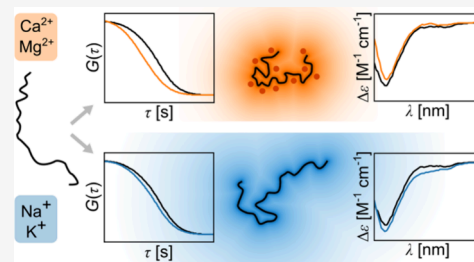
Read Online

ACCESS | Metrics & More | Article Recommendations | Supporting Information

ABSTRACT: Intrinsically disordered proteins (IDPs) respond sensitively to their ionic environment, yet the mechanisms driving ion-induced conformational changes remain incompletely understood. Here, we investigate how counterion valency modulates the dimensions of an extremely charged model IDP, the aspartic and glutamic acid-rich protein AGARP. Fluorescence correlation spectroscopy and size exclusion chromatography reveal a pronounced, valency-dependent reduction in its hydrodynamic radius, with divalent cations (Ca^{2+}, Mg^{2+}) inducing collapse at much lower activities than monovalent cations (Na^+, K^+). Molecular dynamics simulations, direct sampling, and polyampholyte theory quantitatively capture the Debye−Hückel screening by monovalent ions but not the enhanced compaction driven by divalent ion binding thereby suggesting that, beyond differences in screening strength, a valency-sensitive mode of interaction is at play. Circular dichroism spectroscopy shows that compaction occurs without secondary structure formation. Our results demonstrate a structure-free electrostatic collapse and suggest that specific chelation of divalent ions by disordered polyanionic protein chains is a key mechanism regulating IDP compaction, with implications for understanding their behavior in biologically relevant ionic environments.

Intrinsically disordered proteins are essential regulators in diverse biological processes, including cellular signaling,[1,2] gene expression,[3] or biomineralization.[4] Despite their high abundance,[5] our understanding of the determinants of their conformational ensemble equilibria and function remains incomplete.[6] Unlike natively folded proteins, which adopt a singular three-dimensional structure, IDPs exhibit remarkable conformational dynamics and are best studied as rapidly fluctuating ensembles of conformations. IDPs are typically composed of low-complexity sequences, enriched in polar and charged residues and depleted in hydrophobic ones.[7] Thus, their behavior is often described within the frameworks of polyampholyte and polyelectrolyte theories.[8−15] The apparent dimensions of IDP conformational ensembles are usually quantified using the radius of gyration (R_g) or hydrodynamic radius (R_h). These parameters have been shown to vary not only with the protein sequence,[16] but also in response to environmental conditions,[17] such as temperature,[18] pH,[19] osmolality[20] or ionic strength.[21−27] In particular, the effect of solution ionic composition has been examined; in the case of monovalent salts, classical polymer models have demonstrated a high level of agreement with experimental observations of changes in the dimensions of charged proteins due to electrostatic screening.[21,23]

A common assumption about polyelectrolyte or polyampholyte IDPs is that their charges are fully ionized. However, the extent to which the presence of counterions neutralizes ionizable amino acid side chains remains largely unanswered,

despite a long-standing dispute in polymer physics regarding theories for modeling uniformly charged polyelectrolytes.[14] Recently, some studies have addressed the coil−globule transition of IDPs depending on their charge patterning and ionic strength.[28] Although the function of certain IDPs depends on their interactions with divalent ions, particularly the acid-rich proteins involved in biomineralization,[29−32] the effects of these ions on IDP dimensions remain poorly understood. Most prior research has focused on monovalent salts,[21−23] oversimplifying more complex relationships. Consequently, protein-salt interactions are frequently reduced to the effect of electrostatic screening, precluding the ability to address weak but specific counterion recognition.

To address this knowledge gap, we examined the effects of mono- and divalent cations on the hydrodynamic dimensions of the polyanionic aspartic and glutamic acid-rich protein (AGARP)[33] from the coral *Acropora millepora* of the Great Barrier Reef. AGARP is an extremely charged, natively unstructured protein[32] belonging to the family of coral acid-rich proteins (CARPs), which are found in stony corals.[33,29]
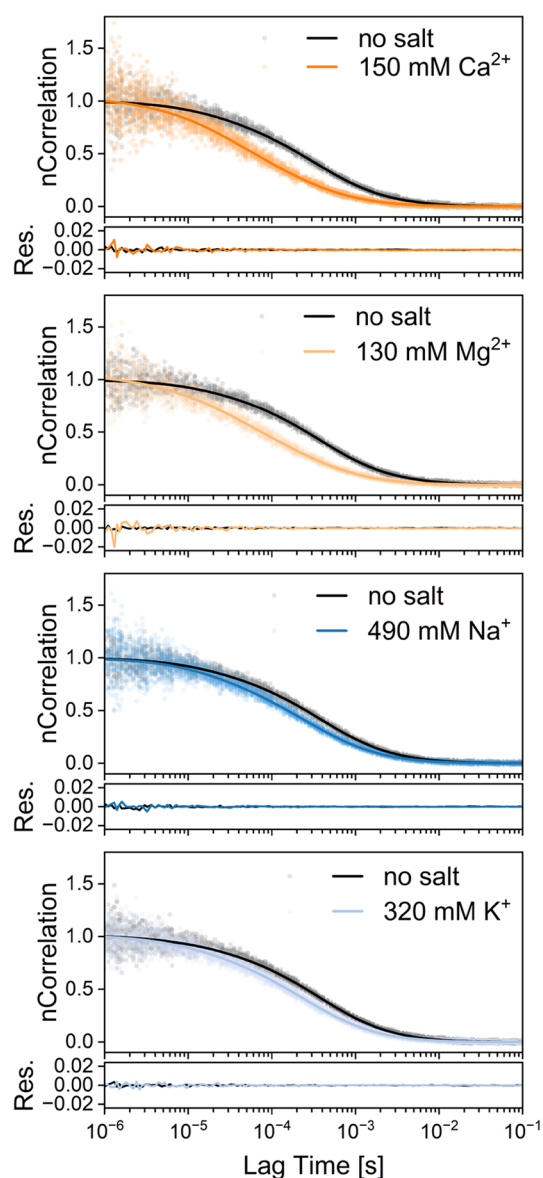
Figure 1. Effects of cations on the self-diffusion of AGARP, measured by FCS. Examples of normalized FCS autocorrelation curves (solid lines) from global fitting to FCS data (translucent points) along with raw fitting residuals for buffers supplemented with $CaCl_2$, $MgCl_2$, NaCl, and KCl (colored lines; ionic strength of 456, 393, 495, or 321 mM including buffer, respectively), compared to reference conditions (black lines; 10 mM Tris, 5% glycerol only). Increasing salt concentration results in shorter diffusion times, indicating more compact AGARP conformations. For experimental details of actual salt concentration determination in the FCS experiment, see Supporting Information.

These proteins are secreted at the organism—seawater interface, where they are thought to regulate the formation of $CaCO_3$ skeletons.[34] Ca^{2+} and Mg^{2+} ions also play a central role in regulating this process, since they directly contribute to aragonite deposition in corals.[35] AGARP was recently shown to undergo liquid—liquid phase separation driven by the interactions with Ca^{2+} under molecular crowding conditions.[32] The AGARP polypeptide chain is composed of 506 amino acid residues, including a total of 212 negatively charged and 65 positively charged residues (Figure S1, Table S1). At pH 8.0, AGARP has a net charge of −148 e per molecule and is devoid
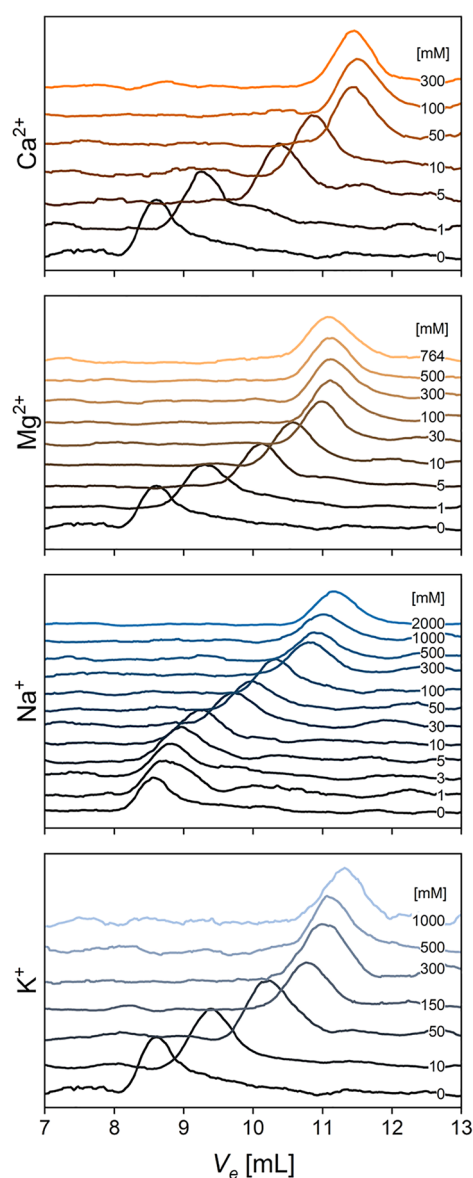

Figure 2. Effects of cations on the diffusion of AGARP through porous medium, measured by SEC. Absorbance signals recorded at 215 nm for runs at increasing salt concentrations ($CaCl_2$, $MgCl_2$, NaCl, and KCl) shown staggered for clarity, with the lowest concentration at the bottom (black) and the highest at the top (colored accordingly with Figure 1). Increasing salt concentration results in larger elution volumes, V_e, indicating slower migration through the column matrix, and thus more compact AGARP conformations.

of folded domains.[32] Thus, AGARP serves as an excellent model protein, with a linear charge density of −0.3 e/residue, which is comparable to that of prothymosin α (−0.4 e/residue). However, AGARP has a much longer chain (506 vs. 111 residues), resulting in greater relative size changes due to the electrostatic self-repulsion.

To elucidate the influence of the environmental electrostatic conditions on the conformational properties of AGARP, we employed a combination of several experimental, numerical, and theoretical approaches. First, we experimentally determined the hydrodynamic radius of AGARP as a function of increasing concentrations of mono- (NaCl, KCl) and divalent ($MgCl_2$, $CaCl_2$) salts using fluorescence correlation spectros-
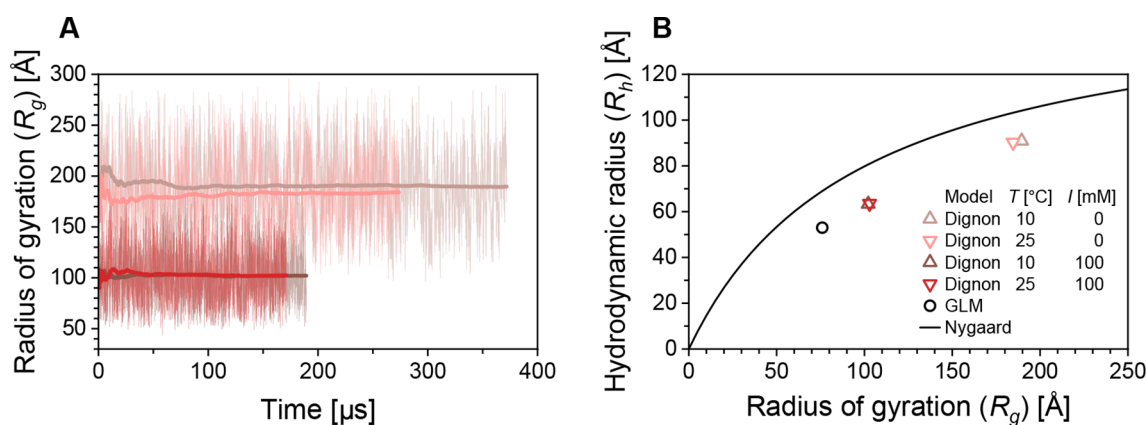
Figure 3. Results of CG MD simulations of AGARP at low (0.001 mM, denoted to as "0", pastel colors) and high (100 mM, saturated colors) ionic strength conditions, at 10 °C (brown) and 25 °C (red). (A) The instantaneous R_g is plotted against simulation time, along with the cumulative average (thicker line). Despite large fluctuations in R_g, a stable long-time average is achieved. (B) Ensembles of conformers from CG MD (red and brown triangles) and MC GLM (black circle) methods were postprocessed using MDA,[37,38] to calculate R_h; the resulting R_h-R_g pairs were compared with the relationship proposed by Nygaard et al.[43] (black curve). The deviation is attributed to more extended configurations of a larger and more highly charged protein than those included in the training data set.[43]

copy (FCS)[36,37] and size exclusion chromatography (SEC) (for details see Supporting Information). Second, we computed the R_h values using Minimum Dissipation Approximation (MDA)[37,38] based on conformers generated by coarse-grained molecular dynamics simulations (CG MD)[39,40] and direct conformational sampling (Globule-Linker Model, GLM).[37] Third, we compared the experimental and numerical results against the theoretical polymer model of Higgs and Joanny.[41] Fourth, we used circular dichroism (CD) spectroscopy to assess whether the counterion-induced compaction of AGARP could be attributed to changes in its secondary structure. We concluded that, surprisingly, the electrostatic collapse of AGARP occurs without protein folding. Finally, we showed that the decrease in the R_h values conforms to the classical Debye−Hückel theory for mono-valent cations. The response of the highly charged protein chain to the presence of divalent salts, by contrast, is additionally enhanced through its specific interactions with the counterions.

The experimental backbone of the presented investigation is formed by measurements obtained using two complementary methods for determining R_h: FCS, which is the only technique that allows for direct measurement of self-diffusion, and SEC. For all experiments, AGARP was purified as previously described[32] and treated with Chelex 100 resin to remove divalent ions. The protein labeled with AF488 (Lumiprobe) was used for FCS, and the unlabeled protein was used for SEC.

FCS measurements were performed essentially as described previously,[36,37] in 30 μL droplets at 25 °C using a titration approach, where aliquots of salt stock solutions in water were sequentially added to a 100 nM protein sample in 10 mM Tris/HCl, 5% glycerol, pH 8.0 (TG buffer), while carefully monitoring evaporation. The evaporation rate was determined prior to titrations by measuring the FCS amplitude for AF488 freely diffusing in the buffer solutions with given salt concentrations. This ensured that the droplet volume was known, which enabled the calculation of the actual salt concentration and the determination of the sample viscosity. A two-component model of 3D diffusion that accounts for residual amounts of free dye in protein samples was fitted to all measurements. The model included a fixed triplet state

relaxation time for AF488 covalently attached to the protein of 2.4 μs as the average lifetime, determined from multiple independent experiments. This allowed us to extract diffusion times and determine the exact R_h of the protein under different conditions.[37] Representative results of the FCS measurements are shown in Figure 1.

Each panel of Figure 1 shows a comparison between the autocorrelation curves for AGARP in the presence of a high salt concentration (colored) and the reference curves recorded without salt (black). The salt concentrations are chosen so that the ionic strength remains comparable across the panels (∼150 mM for divalent salts, orange; ∼450 mM for monovalent salts, blue). In all cases, the autocorrelation curves shift toward noticeably shorter lag times, which indicates faster diffusion and thus a smaller R_h value of the polyelectrolyte in the presence of salts. However, the degree of this salt-induced protein compaction is greater for the divalent salts, as evidenced by the larger shifts to the left on the logarithmic lag time axis. For both mono- and divalent salts, the R_h of AGARP decreases from ∼ 80 Å at low salt concentrations to ∼53 Å at high salt concentrations, with the onset of chain compaction occurring at lower salt concentrations for divalent ions than for monovalent ions.

As a robustness check, we performed analogous measurements using semianalytical SEC as a complementary method. SEC was conducted at 10 °C with detection at 215 nm. Each protein sample, containing AGARP at 4 μM, was incubated for 30 min in TG buffer containing appropriate salt concentration. Prior to each measurement, the column was equilibrated with the corresponding buffer, and the R_h values were determined with experimental uncertainty from the calibration curve (Figure S4).[32]

Consistent with the FCS observations, higher salt concentrations led to an increase in the elution volume (V_e) of the protein in the SEC chromatograms (Figure 2), indicating a more compact conformation and thus longer retention within the porous matrix of the column, with the R_h of AGARP decreasing from ∼113 Å at low salt to ∼58 Å at high salt. SEC, in particular, enabled the measurement of the R_h values at higher salt concentrations—up to 2 M NaCl—than was possible using FCS, due to changes in the optical properties of
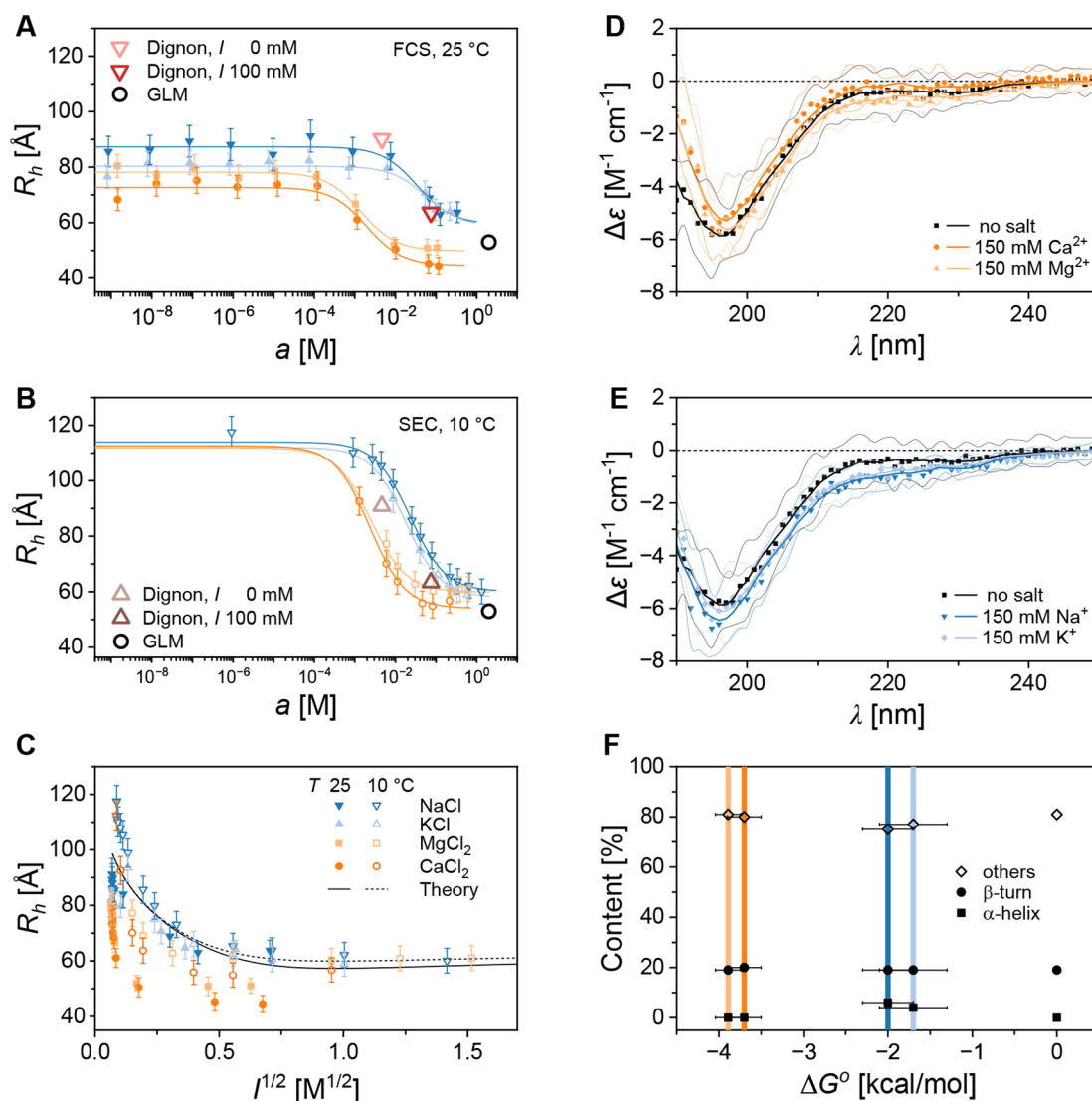
Figure 4. Structure-less electrostatic collapse of AGARP depends on the cation valency. At increasing salt concentrations, the hydrodynamic radius of AGARP, R_h, decreases according to the sigmoidal binding curve (eq 1, Table 1), as evidenced by (A) FCS and (B) SEC. The R_h derived from CG MD (red and brown triangles) and GLM-MDA (black circle) simulations are in line with the experimental trends for the monovalent salts (blue), whereas the divalent salts (orange) induce AGARP compaction at markedly lower salt activities. (C) Combined FCS and SEC data align well with polymer-based Debye−Hückel screening predictions (Theory, continuous and dotted black curves) for monovalent salts, while significant deviations are observed for divalent cations due to the enhanced compaction. Normalized CD spectra of AGARP in the presence of (D) divalent and (E) monovalent salts, analyzed using BeStSel.[50] (F) Results of CD analysis showing negligible α-helix content regardless of the cation type and Gibbs free energy of the binding, ΔG° (Table 1). The β-type structures are indiscernible from random coil (others) in IDPs.[51]

the salt solutions. This revealed saturation of the electrostatic repulsion attenuation effect. At these elevated salt levels, the protein sizes remained largely unchanged regardless of the ion valency.

However, the most salient feature reflecting the strength of interactions between the polyanionic protein chain and counterions is the characteristic range of ion activity at which the compaction occurs. Strikingly, the decrease in the hydrodynamic dimensions observed by FCS was triggered by the divalent cations at the activity ranges that were, on average, approximately 25-fold lower than those for the monovalent cations (∼10-fold lower as seen by SEC). These effects point to more specific interactions between the negatively charged protein chain and Ca^{2+} or Mg^{2+}, since it cannot be explained simply by the higher ionic strength, which, for divalent ions, is multiplied by three.

The experimental results were compared against two types of in silico numerical approaches: CG MD simulations and direct Monte Carlo (MC) sampling (Figure 3). AGARP conformations can range from compact to highly extended, which would require an exceptionally large solvation box, thereby rendering all-atom simulations impractical. To address this limitation, we employed the CG model proposed by Dignon et al.,[39] in which protein conformations are parametrized by the positions of Cα atoms that interact via two types of potentials: screened electrostatic and modified Lennard-Jones. The electrostatic interactions depend on the product of the charges of the interacting residues (Arg, Lys: + 1; Asp, Glu: −1; His: + 0.5; and 0 for other residues), their separation and the Debye screening length, which is computed from the ionic strength of the solution. The modified Lennard-Jones potential corresponds to van der Waals forces and

Table 1. Parameters of Cation Binding by AGARP[a]

	K_d [mM]	ρ	R_0 [Å]	R_{min} [Å]	$\Delta G°$ [kcal/mol]
FCS at 25 °C					
CaCl$_2$	2.0 ± 0.7	−0.39 ± 0.02	72.7 ± 0.9	44.3 ± 1.6	−3.7 ± 0.2
MgCl$_2$	1.4 ± 0.4	−0.362 ± 0.015	78.1 ± 0.6	49.8 ± 1.2	−3.89 ± 0.15
NaCl	34 ± 16	−0.32 ± 0.04	87.3 ± 0.8	59 ± 4	−2.0 ± 0.3
KCl	60 ± 40	−0.27 ± 0.07	80.3 ± 0.8	59 ± 6	−1.7 ± 0.4
SEC at 10 °C					
CaCl$_2$	2.3 ± 0.2	−0.520 ± 0.009	112.6 ± 1.3	54 ± 1.2	−3.41 ± 0.06
MgCl$_2$	2.5 ± 0.3	−0.465 ± 0.008	111.9 ± 1.3	59.9 ± 1.1	−3.38 ± 0.06
NaCl	23 ± 2	−0.473 ± 0.008	113.9 ± 0.8	60.0 ± 1.0	−2.12 ± 0.05
KCl	17.9 ± 1.0	−0.483 ± 0.004	112.1 ± 0.6	58.0 ± 0.5	−2.26 ± 0.03
GLM-MDA				53	

[a]The results of the analysis of AGARP-cation interactions in terms of binding isotherms fitted to FCS or SEC experimental data, within a two-state model assuming identical, non-interacting binding sites and a large excess of cations. K_d, the apparent dissociation constant corresponds to the cation affinity for a single binding site; ρ, the relative difference of the R_h value between the state in the absence of salt, R_0, and the plateau at a high salt activity, where the hydrodynamic radius attains its minimum, R_{min}; $\Delta G°$, the corresponding Gibbs free energy change; in 10 mM Tris/HCl, 5% glycerol, pH 8.0, at 25 °C (FCS) or 10 °C (SEC). The apparent errors are only from numerical fitting. The theoretical R_h value at perfect screening (from GLM-MDA) is shown for comparison.

hydrophobicity, where the interaction strength and interaction range are computed for each pair of residues[39] with further temperature-dependent refinements[40] (see Supporting Information for details). Both types of interactions are truncated at a distance threshold.[39] Simulations were conducted using the user-defined potentials feature of the GROMACS package[42] for at least 150 μs to ensure full equilibration and to obtain precise estimates of both the R_g and R_h values (Figure 3A, solid lines). Such a long simulation period is required due to the substantial thermal fluctuations in the instantaneous R_g, which can vary by as much as 50% (Figure 3A, translucent lines).

The second method of conformer generation was the GLM, as described previously,[37] which operates under the assumption of perfect screening. In this approach, AGARP was modeled as a completely unstructured "linker" chain using a self-avoiding random walk with a steric exclusion range corresponding to the Cα distance.

The ensembles of conformers obtained from both methods were further processed to obtain R_g, and then to calculate R_h using the MDA approach[38] with the hydrodynamic parameters of chain monomers as described earlier[37] (Figure 3B). The R_h vs. R_g pairs obtained were then compared with the predictions proposed by Nygaard et al.[43] The origin of the deviations of our results from their R_h vs. R_g relationship is 3-fold. First, AGARP is an extremely charged IDP, surpassing the charge density range of their original training data set. Second, AGARP is longer (506 residues) than the longest protein in the training data set (450 residues). Third, in the work of Nygaard et al.,[43] the R_h values were computed in a rigid-body approximation,[44,45] which is not well-suited for highly flexible proteins. In contrast, our work uses MDA, which is specifically designed for IDPs and has been validated on a wide range of IDPs.[37] Nevertheless, the Nygaard et al.[43] equation still reproduces the correct trend. The quantitative deviation between the predicted and calculated R_h values can be considered small enough to be make the equation suitable for converting R_g predictions from polymer models to R_h, to facilitate further comparison of experimental results with simulations using analytical expressions.

The measured R_h values were analyzed using two frameworks: apparent direct binding, and a polymer-theoretic approach (Figure 4A-C). In both the FCS and SEC

measurements, the R_h values decreased according to a sigmoidal function of salt activity, a (Figure 4A,B), with plateaus at the extremes of low and high activity. This supports the applicability of a two-state binding model, assuming identical, non-interacting, entropically independent ion-binding sites on a protein molecule and a large excess of ions compared to the number of binding sites. The apparent dissociation constant, K_d, describes the affinity of an ion for a single binding site, while ρ is the observable magnitude of the relative hydrodynamic dimension change due to the binding, according to

$$R_h = R_0\left(1 + \rho\frac{a}{K_d + a}\right) \tag{1}$$

The decrease in R_h, which is indicative of increased AGARP compactness, occurs at much lower activities of divalent ions compared to monovalent ions. As shown in Table 1, the K_d values obtained from FCS and SEC measurements are similar, with differences of one or two standard errors resulting from numerical fitting. The apparent dissociation constants for divalent ions are about several dozen times lower than those for monovalent ions. To facilitate comparison, the values of K_d were converted into the changes in Gibbs free energy ($\Delta G°$) that accompany the ion binding. The $\Delta G°$ values for the Ca^{2+} and Mg^{2+} cations are approximately twice as negative (ca. −4 kcal/mol) as those for the monovalent Na$^+$ and K$^+$ cations (ca. −2 kcal/mol).

Strikingly, the theoretical binding energy of a 3-Å single monovalent salt bridge in a water milieu (ε = 80) is approximately −1.4 kcal/mol, but it can achieve a magnitude 10-fold higher if buried inside a protein hydrophobic core (ε = 8). Depending on water accessibility and entropic contributions due to structure stabilization, the experimentally measured $\Delta G°$ of individual salt bridges ranged from −0.5 and −0.9 kcal/mol for lysozyme-antibody interactions[46] to ca. −3−5 kcal/mol for lysozyme folding.[47] Our $\Delta G°$ values fall in the range that corresponds to salt bridge formation. Considering that the binding involves water-accessible acidic residues, these results imply that the divalent cations are more tightly chelated, while the monovalent cations can only be loosely or transiently coordinated.

Having established the difference in interaction strength between the cations and the protein, we focus on the nature of the interaction in more detail. Contrasting approaches, even in the case of a monovalent salt, have been proposed, whereby some postulate to analyze the interaction as explicit condensation of ions on the protein ionized groups,[48] while others consider the interaction to be spatially diffuse.[21,49] These different modes of interaction can be discerned by quantitative comparison of the experimental results with the predictions of the diffuse Debye–Hückel-like models, where deviations from these predictions would indicate the need to take additional binding mechanisms into account.

While relative changes in the R_h of AGARP upon interaction with ions show little difference between different ions of the same valency using a given method, some differences that reflect the polyelectrolytic nature of the protein are observed between the experimental methods. The relative change measured by SEC appears greater than that observed by FCS. This is primarily driven by the differences at very low salt concentrations, where AGARP adopts highly extended conformations that can affect the reliability of measurements using the Superdex 200 Increase 10/300 GL SEC column, which contains a porous matrix optimized for globular proteins. However, as the chains adopt more compact shapes, this discrepancy disappears. The lower R_h limits, R_{min}, derived from both methods are in excellent agreement and align closely with the GLM-MDA prediction (Table 1, Figure 4A,B).

Next, we compare the experimental results with the model (Figure 4C) applied by Müller-Späth et al.[21] based on the polymer theory of Higgs and Joanny[41] that uses Gaussian displacement statistics to describe the screened electrostatic interaction energy of a chain containing N monomers and a Kuhn length, b. The residues are positively or negatively charged with probabilities f or g. This interaction can be either repulsive or attractive, and its strength depends on the net absolute charge per residue, $f + g$, and the net charge per residue, $f - g$. Both the polyelectrolytic (self-repulsive) and the polyampholytic (self-attractive) interactions noticeably contribute to the theoretical amplitude of the electrostatic collapse. The magnitude of the ampholytic contribution can be examined visually in Figure S7. The second type of interaction considered is the effective excluded volume interaction controlled by the parameter ν, which is the only fitting parameter of the model. The screening length, λ_D, is assumed to follow the Debye–Hückel dependence on ionic strength, I, and the Bjerrum length, l_B, which combines the properties of the liquid and temperature.

The polyampholyte model is described by the following relations:

$$R_g = \frac{\alpha b}{\sqrt{6}} N^{1/2} \tag{2}$$

$$\alpha^5 = \alpha^3 + \left(\frac{6N}{\pi^3}\right)^{1/2} \nu^* \tag{3}$$

$$\nu^* = \nu + \frac{\pi l_B^3}{b^3}\left(4(f-g)^2 \frac{\lambda_D^2}{l_B^2} - (f+g)^2 \frac{\lambda_D}{l_B}\right) \tag{4}$$

$$\lambda_D = (8\pi l_B N_A I)^{-1/2} \tag{5}$$

In the presented cases, assuming $2 < \alpha < 5$ and omitting α^3 term in eq 3 leads to an approximation error of at most 5%

when determining R_g. Care is needed when using this approximation, as it hinges on large values of α; at the same time large α values correspond to large λ_D or small ionic strengths where the Higgs and Joanny approaches its limits of applicability due to divergence of interaction terms. These issues do not manifest in the data presented herein because of the minimal ionic strength of *ca.* half ionized 10 mM Tris present in all experiments. As such, λ_D never exceeds ~ 50 Å, which is comparable with the protein size, allowing for both the use of the Higgs and Joanny model and the convenient approximation. The values of the constants are listed in the Supporting Information (Table S1). The R_g predictions were combined with the phenomenological relationship established by Nygaard et al.[43] to determine R_h:

$$R_h = R_g\left(\alpha_3 + \frac{\alpha_1(R_g - \alpha_2 N^{0.33})}{N^{0.6} - N^{0.33}}\right)^{-1} \tag{6}$$

with α_i parameter values as described therein. The combined eqs 2−5 and 6 were used in the fitting procedure to determine ν from either FCS and SEC measurements with monovalent salts, which resulted in similar values of $\nu = 2.42$ and $\nu = 2.87$, respectively.

Figure 4C shows that the polyampholyte theory model adequately describes the electrostatic compaction of AGARP induced by screening by monovalent ions. However, it fails to account for the stronger collapse upon interactions with divalent ions. This further supports the possibility of tight binding in the latter case. The presented methodology for establishing additional binding effects is akin to that of Ruggeri et al.,[49] whereby a model of the decrease in apparent charge was sought. Therein, the traditional screening model was sufficient to describe the interaction of counterions with prothymosin α, accounting for a 35% decrease in measured charge relative to structural charge. Likewise, in our work, we observe effects of diffuse interaction with monovalent salts. It should be underscored that this is not in contradiction with earlier analyses using the apparent binding model; rather, it represents a refinement that allows investigation of the mode of interaction, not merely the presence thereof. In contrast, Ca^{2+} and Mg^{2+} observations do not align with these simple predictions, and thus diffuse, Debye-like interaction alone is insufficient to explain their behavior.

To test whether the observed $\sim 40\%$ decrease in the hydrodynamic dimensions of AGARP (Table 1) is linked to the protein folding, CD spectra were recorded in a TG buffer supplemented with 150 mM salts and without added salt. The CD spectra of AGARP in the presence of di- (Figure 4D) and monovalent (Figure 4E) cations are almost identical to those under salt-free conditions, displaying only slight changes at 190 and 218 nm, respectively, that are hardly interpretable in terms of the quantitative contributions of secondary structure elements. The BeStSel[50] analysis revealed that cations, regardless of valency, do not induce the formation of measurable amounts of α-helices (Figure 4F, Table S2), the only type of secondary structure that can be reliably quantified by CD in the case of IDPs.[51] We thus conclude that AGARP compaction caused by both Debye−Hückel screening of electrostatic repulsion and additional enhancement by chelation of divalent ions is a conformational collapse that preserves the disordered state of the protein.

Our results are in line with the previously reported changes in IDP sizes due to screening-induced collapse for the

polyelectrolytic IDP prothymosin α[21] in the presence of monovalent salts. Similarly to AGARP, the collapse of prothymosin α can be described by polymeric theories of Debye screening. The amplitude of this effect (30%), however, is smaller than that for AGARP (40%), despite the slightly higher charge density of prothymosin α. *In silico* studies have also shown that prothymosin α responds selectively to divalent ions,[27] but this result has yet to be confirmed experimentally. Collapse under the influence of divalent ions, without accompanying secondary structure formation, analogous to AGARP, has been demonstrated experimentally for other polyanionic proteins associated with biomineralization, such as the otolith matrix macromolecule-64 (OMM-64)[31] and Starmaker.[30] Although these proteins are similar to AGARP in terms of chain length (608 and 593 residues for OMM-64 and Starmaker, respectively) their smaller charge density (-0.27 and -0.23 e/res, respectively) results in a decreased electrostatic collapse amplitude (~12% and 30%, respectively) compared to AGARP. These characteristics of polyelectrolytes contrast with the features of polyampholytic proteins, such as, e.g., the basic helix−loop−helix family,[23] exhibiting the opposite effect of screening-induced swelling at relatively low, physiological monovalent salt concentrations.

Guided by the observations of the structure-free, counterion-induced collapse of AGARP, we propose the following schematic representation of this phenomenon for acid-rich proteins (Figure 5). The absence of salt favors extended protein conformations with high R_h values. As the salt concentration increases, a cloud of counterions forms around the protein, suppressing intraprotein electrostatic repulsion, and resulting in relaxed, more compact conformations described by lower R_h values. The strength of this effect is captured by the Debye screening length for monovalent salts. On the other hand, the screening effect, despite being three times stronger for divalent salts at the same molar concentration, is insufficient to explain the dramatic collapse of R_h triggered by divalent salts. We propose that a kind of more specific binding is necessary to explain the favoring of more compact conformations in the presence of Ca^{2+} or Mg^{2+}.

None of the canonical Ca^{2+}-binding motifs, such as EF-hand[52,53] or Excalibur,[54,55] could be identified by InterPro[56] in the AGARP sequence. The protein exhibits an approximately uniform distribution of short condensed-charge motifs,[57] with acidic residues primarily forming doublets or triplets, with one 7-residue-long condensed-charge motif (Figure S8). This observation leads us to postulate a chelation-like binding mode, reminiscent of how EDTA coordinates divalent cations[58,59] through four carboxylate groups from Asp or Glu side chains, but much weaker, due to entropic reasons for a long protein chain. Interestingly, the quantitative dependence of the collapse effect as a function of Ca^{2+} and Mg^{2+} activity is well explained by the apparent binding model, with the P-values from runs test from 0.26 to 0.96. This means that identical, non-interacting, entropically independent ion-binding sites on the protein molecule are a good first approximation of the binding mode.

The millimolar affinity of AGARP to both Ca^{2+} and Mg^{2+} cations is much weaker than that of, *e.g.*, mammalian intrinsically disordered extracellular matrix protein involved in biomineralization, osteopontin (OPN).[60] The affinity of OPN for Ca^{2+} was determined by isothermal titration calorimetry as $K_d \sim 35$ nM with the number of identical, non-interacting sites of ~ 10, while K_d for Mg^{2+} was ~ 2 μM with ~ 13 binding sites. OPN is less acidic (pI 4.46) and half as long (262 residues without the signal sequence) as AGARP (pI 3.94, 506 residues). However, its amino acid composition is more biased toward aspartic acid residues, with an Asp:Glu ratio of 1.30 vs. 0.88 for AGARP, which may also partially explain the difference in the affinity.[57] Thus, AGARP can serve as a good model to test the polymeric behavior of highly charged IDPs at the limit of low affinity counterion interactions.

Moreover, we show that the compaction of the natively unstructured, acid-rich AGARP is a process of structure-less collapse. This is supported by two observations: first, CD spectra show a negligible amount of the α-helix content (Figure 4D-F, Table S2); second, the minima of the R_h values under both divalent and monovalent salt conditions align with the GLM-MDA's self-avoiding random walk predictions (Table 1). Furthermore, the correspondence of the R_h minimal values supports the postulate of local Ca^{2+} or Mg^{2+} binding without formation of long-range secondary structures.

In this work, using the large polyanionic IDP AGARP as a model, we provide both experimental and theoretical evidence that unstructured proteins can interact weakly but specifically with counterions, distinguishing between their valencies, as robustly established by two experimental methods analyzed using the apparent binding model. By quantitatively comparing the dependence of hydrodynamic size with a reference theoretical and numerical calculations, we establish additionally that increased screening potency of divalent salts is insufficient to explain this difference. We demonstrate
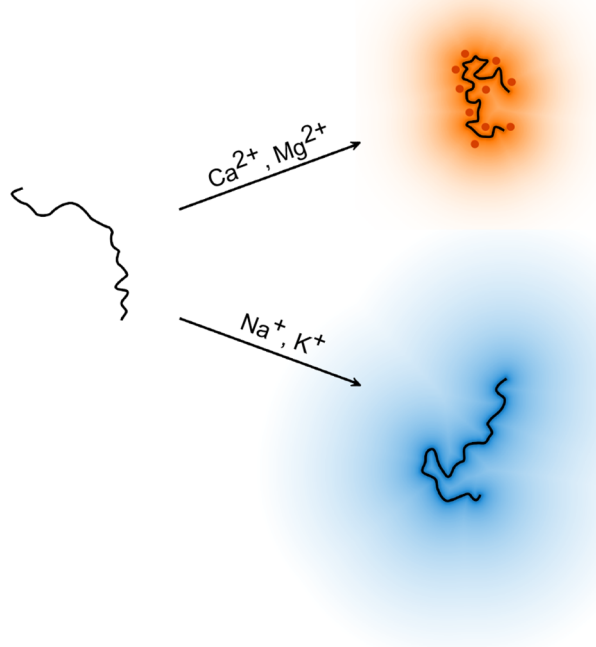

Figure 5. Schematic representation of the enhancement of the electrostatic collapse of an acid-rich protein induced by divalent cations. In a solution of low ionic strength (left), AGARP (black line) adopts extended conformations due to intraprotein repulsion. In the presence of monovalent cations, the repulsion is screened by the surrounding cation cloud (bottom right; blue gradient). In contrast, divalent cations bind more specifically, yielding more effective charge neutralization (top right; red points, orange gradient).

additional chelating protein behavior in the presence of divalent cations such as Ca^{2+} and Mg^{2+}, in contrast to the simple electrostatic screening observed for monovalent cations like Na^+ and K^+. Even upon saturation with counterions, AGARP does not develop secondary structures.

The chain compaction caused by single Ca^{2+} ions can bridge two or more negatively charged AGARP side chains, resembling the chelation of cations by EDTA or EGTA, but with much weaker strength due to non-optimal geometry and the need of the protein chain reconfiguration. Moreover, we have recently observed the aggregation of AGARP molecules at a submicromolar concentration upon contact with Ca^{2+} ions during diffusion through a confocal volume, leading to the deposition of amorphous calcium carbonate,[32] which means that the overall protein charge had to be neutralized by counterions. For this study, however, we excluded all fluorescence count rate spikes reflecting the aggregation events from the FCS analysis to obtain the hydrodynamic dimensions of solely monomeric protein chains. Thus, inferring the total neutralization of the protein charge by the direct counterion binding to the chain at the titration saturation plateau would not be entirely justified here. On the other hand, the need to use a low protein concentration to prevent the aggregation hinders the ability to determine the exact number of binding sites using ITC or to measure the actual charge based on the ζ-potential.[61]

We conclude that the IDP undergoes a structure-less electrostatic collapse, a conformational compaction driven by suppression of electrostatic self-repulsion without folding. Our findings suggest that a comprehensive understanding of charged IDP–counterion interactions requires moving beyond the conceptual framework of ion clouds, particularly given the critical role of divalent Ca^{2+} and Mg^{2+} cations in the biological function of acid-rich proteins in regulating biomineralization.

■ ASSOCIATED CONTENT

Data Availability Statement

The raw data are deposited on the RepOD data server with the following DOI: https://doi.org/10.18150/7DLIT3.

Ⓢ Supporting Information

The Supporting Information is available free of charge at https://pubs.acs.org/doi/10.1021/acs.jpclett.5c02098.

> Materials and Methods, Additional Tables (list of parameters, BeStSel CD analysis results, limiting molar conductivity from SEC), and Figures (bioinformatics analysis of AGARP, count rates from FCS, SEC calibration curve, conductivity from SEC) (PDF)
>
> Transparent Peer Review report available (PDF)

■ AUTHOR INFORMATION

Corresponding Author

Anna Niedzwiecka − *Laboratory of Biological Physics, Institute of Physics, Polish Academy of Sciences, PL-02668 Warsaw, Poland;* Ⓞ orcid.org/0000-0001-5208-0733; Email: annan@ifpan.edu.pl

Authors

Barbara P. Klepka − *Laboratory of Biological Physics, Institute of Physics, Polish Academy of Sciences, PL-02668 Warsaw, Poland;* Ⓞ orcid.org/0000-0002-4496-8713

Radost Waszkiewicz − *Laboratory of Biological Physics, Institute of Physics, Polish Academy of Sciences, PL-02668*

Warsaw, Poland; Present Address: Institute of Physics and Astronomy, University of Potsdam, Karl-Liebknecht-Strasse 24/25, 14476 Potsdam-Golm, Germany; Ⓞ orcid.org/0000-0002-0376-1708

Michał Wojciechowski − *Laboratory of Biological Physics, Institute of Physics, Polish Academy of Sciences, PL-02668 Warsaw, Poland;* Ⓞ orcid.org/0000-0002-1966-9877

Agnieszka Michaś − *Laboratory of Biological Physics, Institute of Physics, Polish Academy of Sciences, PL-02668 Warsaw, Poland;* Ⓞ orcid.org/0000-0002-7005-4368

Complete contact information is available at:
https://pubs.acs.org/10.1021/acs.jpclett.5c02098

Author Contributions

B.P.K. and A.N. designed and performed the experiments; M.W designed and performed the *in silico* simulations; R.W. designed and performed the theoretical calculations; B.P.K., R.W., M.W., and A.N. analyzed, interpreted, and visualized the data; B.P.K., R.W., and A.N. wrote the manuscript, with contributions from the other authors; A.M. did preliminary experiments; A.N. acquired the funding and conceived, designed, and supervised the project. All authors have approved the final version of the manuscript.

Notes

The authors declare no competing financial interest.

■ REFERENCES

(1) Wright, P. E.; Dyson, H. J. Intrinsically Disordered Proteins in Cellular Signaling and Regulation. *Nat. Rev. Mol. Cell Biol.* **2015**, *16* (1), 18−29.

(2) Bondos, S. E.; Dunker, A. K.; Uversky, V. N. Intrinsically Disordered Proteins Play Diverse Roles in Cell Signaling. *Cell Commun. Signal* **2022**, *20* (1), 20.

(3) Ferrie, J. J.; Karr, J. P.; Tjian, R.; Darzacq, X. "Structure"-Function Relationships in Eukaryotic Transcription Factors: The Role of Intrinsically Disordered Regions in Gene Regulation. *Mol. Cell* **2022**, *82* (21), 3970−3984.

(4) Evans, J. S. The Biomineralization Proteome: Protein Complexity for a Complex Bioceramic Assembly Process. *Proteomics* **2019**, *19* (16), No. 1900036.

(5) Ward, J. J.; Sodhi, J. S.; McGuffin, L. J.; Buxton, B. F.; Jones, D. T. Prediction and Functional Analysis of Native Disorder in Proteins from the Three Kingdoms of Life. *J. Mol. Biol.* **2004**, *337* (3), 635−645.

(6) Dyson, H. J.; Wright, P. E. Intrinsically Unstructured Proteins and Their Functions. *Nat. Rev. Mol. Cell Biol.* **2005**, *6* (3), 197−208.

(7) Uversky, V. N.; Gillespie, J. R.; Fink, A. L. Why Are "Natively Unfolded" Proteins Unstructured under Physiologic Conditions? *Proteins* **2000**, *41* (3), 415−427.

(8) Ha, B. Y.; Thirumalai, D. Conformations of a Polyelectrolyte Chain. *Phys. Rev. A* **1992**, *46* (6), R3012−R3015.

(9) Stevens, M. J. Simulation of Polyelectrolytes: Counterion Condensation, Ion Capture, and Bundle Binding. *AIP Conf Proc.* **1999**, *492* (1), 265−280.

(10) Liu, S.; Muthukumar, M. Langevin Dynamics Simulation of Counterion Distribution around Isolated Flexible Polyelectrolyte Chains. *J. Chem. Phys.* **2002**, *116* (22), 9975−9982.

(11) Muthukumar, M. Theory of Counter-Ion Condensation on Flexible Polyelectrolytes: Adsorption Mechanism. *J. Chem. Phys.* **2004**, *120* (19), 9343−9350.

(12) Lee, C.-L.; Muthukumar, M. Phase Behavior of Polyelectrolyte Solutions with Salt. *J. Chem. Phys.* **2009**, *130* (2), No. 024904.

(13) Araki, T. Conformational Changes of Polyelectrolyte Chains in Solvent Mixtures. *Soft Matter* **2016**, *12* (28), 6111−6119.

(14) Muthukumar, M. 50th Anniversary Perspective: A Perspective on Polyelectrolyte Solutions. *Macromolecules* **2017**, *50* (24), 9528−9560.

(15) Lin, Y.-H.; Brady, J. P.; Chan, H. S.; Ghosh, K. A Unified Analytical Theory of Heteropolymers for Sequence-Specific Phase Behaviors of Polyelectrolytes and Polyampholytes. *J. Chem. Phys.* **2020**, *152* (4), No. 045102.

(16) Mao, A. H.; Crick, S. L.; Vitalis, A.; Chicoine, C. L.; Pappu, R. V. Net Charge per Residue Modulates Conformational Ensembles of Intrinsically Disordered Proteins. *P Natl. Acad. Sci. USA* **2010**, *107* (18), 8183−8188.

(17) Uversky, V. N. Intrinsically Disordered Proteins and Their Environment: Effects of Strong Denaturants, Temperature, pH, Counter Ions, Membranes, Binding Partners, Osmolytes, and Macromolecular Crowding. *Protein J.* **2009**, *28* (7), 305−325.

(18) Langridge, T. D.; Tarver, M. J.; Whitten, S. T. Temperature Effects on the Hydrodynamic Radius of the Intrinsically Disordered N-Terminal Region of the P53 Protein. *Proteins* **2014**, *82* (4), 668−678.

(19) Uversky, V. N.; Gillespie, J. R.; Millett, I. S.; Khodyakova, A. V.; Vasiliev, A. M.; Chernovskaya, T. V.; Vasilenko, R. N.; Kozlovskaya, G. D.; Dolgikh, D. A.; Fink, A. L.; Doniach, S.; Abramov, V. M. Natively Unfolded Human Prothymosin α Adopts Partially Folded Collapsed Conformation at Acidic pH. *Biochemistry* **1999**, *38* (45), 15009−15016.

(20) Moses, D.; Yu, F.; Ginell, G. M.; Shamoon, N. M.; Koenig, P. S.; Holehouse, A. S.; Sukenik, S. Revealing the Hidden Sensitivity of Intrinsically Disordered Proteins to Their Chemical Environment. *J. Phys. Chem. Lett.* **2020**, *11* (23), 10131−10136.

(21) Muller-Spath, S.; Soranno, A.; Hirschfeld, V.; Hofmann, H.; Ruegger, S.; Reymond, L.; Nettels, D.; Schuler, B. Charge Interactions Can Dominate the Dimensions of Intrinsically Disordered Proteins. *P Natl. Acad. Sci. USA* **2010**, *107* (33), 14609−14614.

(22) Hofmann, H.; Soranno, A.; Borgia, A.; Gast, K.; Nettels, D.; Schuler, B. Polymer Scaling Laws of Unfolded and Intrinsically Disordered Proteins Quantified with Single-Molecule Spectroscopy. *P Natl. Acad. Sci. USA* **2012**, *109* (40), 16155−16160.

(23) Vancraenenbroeck, R.; Harel, Y. S.; Zheng, W.; Hofmann, H. Polymer Effects Modulate Binding Affinities in Disordered Proteins. *P Natl. Acad. Sci. USA* **2019**, *116* (39), 19506−19512.

(24) Wohl, S.; Jakubowski, M.; Zheng, W. Salt-Dependent Conformational Changes of Intrinsically Disordered Proteins. *J. Phys. Chem. Lett.* **2021**, *12* (28), 6684−6691.

(25) Maity, H.; Baidya, L.; Reddy, G. Salt-Induced Transitions in the Conformational Ensembles of Intrinsically Disordered Proteins. *J. Phys. Chem. B* **2022**, *126* (32), 5959−5971.

(26) Liu, Z.; Thirumalai, D. Impact of Guanidinium Hydrochloride on the Shapes of Prothymosin-α and α-Synuclein Is Dramatically Different. *Biochemistry* **2025**, *64* (1), 105−113.

(27) Baidya, L.; Maity, H.; Reddy, G. Salts Influence IDP Properties by Modulating the Population of Conformational Clusters. *J. Phys. Chem. B* **2025**, *129* (9), 2433−2445.

(28) Huihui, J.; Firman, T.; Ghosh, K. Modulating Charge Patterning and Ionic Strength as a Strategy to Induce Conformational Changes in Intrinsically Disordered Proteins. *J. Chem. Phys.* **2018**, *149* (8), No. 085101.

(29) Mass, T.; Drake, J. L.; Haramaty, L.; Kim, J. D.; Zelzion, E.; Bhattacharya, D.; Falkowski, P. G. Cloning and Characterization of Four Novel Coral Acid-Rich Proteins That Precipitate Carbonates in Vitro. *Curr. Biol.* **2013**, *23* (12), 1126−1131.

(30) Wojtas, M.; Hołubowicz, R.; Poznar, M.; Maciejewska, M.; Ożyhar, A.; Dobryszycki, P. Calcium Ion Binding Properties and the Effect of Phosphorylation on the Intrinsically Disordered Starmaker Protein. *Biochemistry* **2015**, *54* (42), 6525−6534.

(31) Poznar, M.; Hołubowicz, R.; Wojtas, M.; Gapiński, J.; Banachowicz, E.; Patkowski, A.; Ożyhar, A.; Dobryszycki, P. Structural Properties of the Intrinsically Disordered, Multiple Calcium Ion-Binding Otolith Matrix Macromolecule-64 (OMM-64). *BBA-Proteins Proteom* **2017**, *1865* (11), 1358−1371.

(32) Klepka, B. P.; Michaś, A.; Wojciechowski, T.; Niedzwiecka, A. Biomineralization Controlled by Liquid−Liquid Phase Separation of a Highly Charged Protein. *Small*, **2025**, .

(33) Ramos-Silva, P.; Kaandorp, J.; Huisman, L.; Marie, B.; Zanella-Cléon, I.; Guichard, N.; Miller, D. J.; Marin, F. The Skeletal Proteome of the Coral Acropora Millepora: The Evolution of Calcification by Co-Option and Domain Shuffling. *Mol. Biol. Evol.* **2013**, *30* (9), 2099−2112.

(34) Drake, J. L.; Mass, T.; Stolarski, J.; Von Euw, S.; van de Schootbrugge, B.; Falkowski, P. G. How Corals Made Rocks through the Ages. *Glob Change Biol.* **2020**, *26* (1), 31−53.

(35) Mollica, N. R.; Guo, W.; Cohen, A. L.; Huang, K.-F.; Foster, G. L.; Donald, H. K.; Solow, A. R. Ocean Acidification Affects Coral Growth by Reducing Skeletal Density. *P Natl. Acad. Sci. USA* **2018**, *115* (8), 1754−1759.

(36) Białobrzewski, M. K.; Klepka, B. P.; Michaś, A.; Cieplak-Rotowska, M. K.; Staszałek, Z.; Niedźwiecka, A. Diversity of Hydrodynamic Radii of Intrinsically Disordered Proteins. *Eur. Biophys J.* **2023**, *52* (6), 607−618.

(37) Waszkiewicz, R.; Michaś, A.; Białobrzewski, M. K.; Klepka, B. P.; Cieplak-Rotowska, M. K.; Staszałek, Z.; Cichocki, B.; Lisicki, M.; Szymczak, P.; Niedzwiecka, A. Hydrodynamic Radii of Intrinsically Disordered Proteins: Fast Prediction by Minimum Dissipation Approximation and Experimental Validation. *J. Phys. Chem. Lett.* **2024**, *15* (19), 5024−5033.

(38) Cichocki, B.; Rubin, M.; Niedzwiecka, A.; Szymczak, P. Diffusion Coefficients of Elastic Macromolecules. *J. Fluid Mech.* **2019**, *878*, R3.

(39) Dignon, G. L.; Zheng, W.; Kim, Y. C.; Best, R. B.; Mittal, J. Sequence Determinants of Protein Phase Behavior from a Coarse-Grained Model. *PLoS Comput. Biol.* **2018**, *14* (1), No. e1005941.

(40) Dignon, G. L.; Zheng, W.; Kim, Y. C.; Mittal, J. Temperature-Controlled Liquid-Liquid Phase Separation of Disordered Proteins. *ACS Cent Sci.* **2019**, *5* (5), 821−830.

(41) Higgs, P. G.; Joanny, J. Theory of Polyampholyte Solutions. *J. Chem. Phys.* **1991**, *94* (2), 1543−1554.

(42) Pronk, S.; Páll, S.; Schulz, R.; Larsson, P.; Bjelkmar, P.; Apostolov, R.; Shirts, M. R.; Smith, J. C.; Kasson, P. M.; van der Spoel, D.; Hess, B.; Lindahl, E. GROMACS 4.5: A High-Throughput and Highly Parallel Open Source Molecular Simulation Toolkit. *Bioinformatics* **2013**, *29* (7), 845−854.

(43) Nygaard, M.; Kragelund, B. B.; Papaleo, E.; Lindorff-Larsen, K. An Efficient Method for Estimating the Hydrodynamic Radius of Disordered Protein Conformations. *Biophys. J.* **2017**, *113* (3), 550−557.

(44) García de la Torre, J.; Huertas, M. L.; Carrasco, B. Calculation of Hydrodynamic Properties of Globular Proteins from Their Atomic-Level Structure. *Biophys. J.* **2000**, *78* (2), 719−730.

(45) Ortega, A.; Amorós, D.; García de la Torre, J. Prediction of Hydrodynamic and Other Solution Properties of Rigid Proteins from Atomic- and Residue-Level Models. *Biophys. J.* **2011**, *101* (4), 892−898.

(46) Shiroishi, M.; Yokota, A.; Tsumoto, K.; Kondo, H.; Nishimiya, Y.; Horii, K.; Matsushima, M.; Ogasahara, K.; Yutani, K.; Kumagai, I.

Structural Evidence for Entropic Contribution of Salt Bridge Formation to a Protein Antigen-Antibody Interaction: The Case of Hen Lysozyme-HyHEL-10 Fv Complex. *J. Biol. Chem.* **2001**, *276* (25), 23042−23050.

(47) Anderson, D. E.; Becktel, W. J.; Dahlquist, F. W. pH-Induced Denaturation of Proteins: A Single Salt Bridge Contributes 3−5 kcal/Mol to the Free Energy of Folding of T4 Lysozyme. *Biochemistry* **1990**, *29* (9), 2403−2408.

(48) Phillips, M.; Muthukumar, M.; Ghosh, K. Beyond Monopole Electrostatics in Regulating Conformations of Intrinsically Disordered Proteins. *PNAS Nexus* **2024**, *3* (9), No. pgae367.

(49) Ruggeri, F.; Zosel, F.; Mutter, N.; Różycka, M.; Wojtas, M.; Ożyhar, A.; Schuler, B.; Krishnan, M. Single-Molecule Electrometry. *Nat. Nanotechnol* **2017**, *12* (5), 488−495.

(50) Micsonai, A.; Moussong, É.; Wien, F.; Boros, E.; Vadászi, H.; Murvai, N.; Lee, Y.-H.; Molnár, T.; Réfrégiers, M.; Goto, Y.; Tantos, Á.; Kardos, J. BeStSel: Webserver for Secondary Structure and Fold Prediction for Protein CD Spectroscopy. *Nucleic Acids Res.* **2022**, *50* (W1), W90−W98.

(51) Micsonai, A.; Moussong, É.; Murvai, N.; Tantos, Á.; Tőke, O.; Réfrégiers, M.; Wien, F.; Kardos, J. Disordered-Ordered Protein Binary Classification by Circular Dichroism Spectroscopy. *Front Mol. Biosci* **2022**, *9*, No. 863141.

(52) Kretsinger, R. H. Calcium-Binding Proteins. *Annu. Rev. Biochem.* **1976**, *45*, 239−266.

(53) Zhou, Y.; Yang, W.; Kirberger, M.; Lee, H.-W.; Ayalasomayajula, G.; Yang, J. J. Prediction of EF-Hand Calcium-Binding Proteins and Analysis of Bacterial EF-Hand Proteins. *Proteins* **2006**, *65* (3), 643−655.

(54) Vyas, N. K.; Vyas, M. N.; Quiocho, F. A. A Novel Calcium Binding Site in the Galactose-Binding Protein of Bacterial Transport and Chemotaxis. *Nature* **1987**, *327* (6123), 635−638.

(55) Rigden, D. J.; Jedrzejas, M. J.; Galperin, M. Y. An Extracellular Calcium-Binding Domain in Bacteria with a Distant Relationship to EF-Hands. *FEMS Microbiol Lett.* **2003**, *221* (1), 103−110.

(56) Blum, M.; Andreeva, A.; Florentino, L. C.; Chuguransky, S. R.; Grego, T.; Hobbs, E.; Pinto, B. L.; Orr, A.; Paysan-Lafosse, T.; Ponamareva, I.; Salazar, G. A.; Bordin, N.; Bork, P.; Bridge, A.; Colwell, L.; Gough, J.; Haft, D. H.; Letunic, I.; Llinares-López, F.; Marchler-Bauer, A.; Meng-Papaxanthos, L.; Mi, H.; Natale, D. A.; Orengo, C. A.; Pandurangan, A. P.; Piovesan, D.; Rivoire, C.; Sigrist, C. J. A.; Thanki, N.; Thibaud-Nissen, F.; Thomas, P. D.; Tosatto, S. C. E.; Wu, C. H.; Bateman, A. InterPro: The Protein Sequence Classification Resource in 2025. *Nucleic Acids Res.* **2025**, *53* (D1), D444−D456.

(57) Newcombe, E. A.; Fernandes, C. B.; Lundsgaard, J. E.; Brakti, I.; Lindorff-Larsen, K.; Langkilde, A. E.; Skriver, K.; Kragelund, B. B. Insight into Calcium-Binding Motifs of Intrinsically Disordered Proteins. *Biomolecules* **2021**, *11* (8), 1173.

(58) Stezowski, J. J.; Countryman, R.; Hoard, J. L. Structure of the Ethylenediaminetetracetatoaquomagnesate(II) Ion in a Crystalline Sodium Salt. Comparative Stereochemistry of the Seven-Coordinate Chelates of Magnesium(II), Manganese(II), and Iron(III). *Inorg. Chem.* **1973**, *12* (8), 1749−1754.

(59) Atkins, P.; Overton, T.; Rourke, J.; Weller, M.; Armstrong, F. An Introduction to Coordination Compounds. In *Shriver and Atkins' Inorganic Chemistry*; Oxford University Press: Oxford, U.K., 2010.

(60) Klaning, E.; Christensen, B.; Sørensen, E. S.; Vorup-Jensen, T.; Jensen, J. K. Osteopontin Binds Multiple Calcium Ions with High Affinity and Independently of Phosphorylation Status. *Bone* **2014**, *66*, 90−95.

(61) Crabtree, M. D.; Holland, J.; Pillai, A. S.; Kompella, P. S.; Babl, L.; Turner, N. N.; Eaton, J. T.; Hochberg, G. K. A.; Aarts, D. G. A. L.; Redfield, C.; Baldwin, A. J.; Nott, T. J. Ion Binding with Charge Inversion Combined with Screening Modulates DEAD Box Helicase Phase Transitions. *Cell Rep* **2023**, *42* (11), No. 113375.